A Multidisciplinary Approach to Probing Enthalpy–Entropy Compensation and the Interfacial Mobility Model

Erin M. Wilfong,[†] Yuri Kogiso,[‡] Sivaramakrishnan Muthukrishnan,[‡] Thomas Kowatz,[§] Yu Du,[†] Amber Bowie,[†] James H. Naismith,[§] Christopher M. Hadad,[‡] Eric J. Toone,[†] and Terry L. Gustafson*,[‡]

[†]Department of Chemistry, Duke University, Durham, North Carolina 27708, United States

[‡]Department of Chemistry, The Ohio State University, 100 West 18th Avenue, Columbus, Ohio 43210, United States

[§]Biomedical Sciences Research Complex, The University, St. Andrews, Fife KY16 9ST, Scotland, United Kingdom

S *Supporting Information*

ABSTRACT: In recent years, interfacial mobility has gained popularity as a model with which to rationalize both affinity in ligand binding and the often observed phenomenon of enthalpy–entropy compensation. While protein contraction and reduced mobility, as demonstrated by computational and NMR techniques respectively, have been correlated to entropies of binding for a variety of systems, to our knowledge, Raman difference spectroscopy has never been included in these analyses. Here, nonresonance Raman difference spectroscopy, isothermal titration calorimetry, and X-ray crystallography were utilized to correlate protein contraction, as demonstrated by an increase in protein interior packing and decreased residual protein movement, with trends of enthalpy–entropy compensation. These results are in accord with the interfacial mobility model and lend additional credence to this view of protein activity.
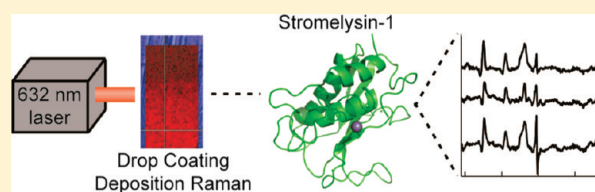
■ INTRODUCTION

Molecular association lies at the center of virtually all biological processes. Enzymes bind their substrates to catalyze important biochemical transformations; ribosomes bind both tRNAs and mRNA to facilitate protein translation. Despite the ubiquity of biological binding, the underlying principles governing these interactions remain obscure. An understanding of molecular associations is further complicated by several poorly understood binding phenomena such as additivity, enthalpy–entropy compensation, and the molecular nature of hydrophobic dissolution.

Among the most frequently observed and poorly understood phenomena is enthalpy–entropy compensation, or large offsetting changes in enthalpy and entropy in response to modification in protein or ligand structure. In an effort to rationalize enthalpy–entropy compensation in carbonic anhydrase, Whitesides and co-workers suggested that ligand binding might be driven by tightening of the protein–ligand interface, a concept termed the interfacial mobility.[1] The basis of this theory is that tightening of the ligand–protein interface maximizes enthalpic intermolecular forces (ionic, van der Waals, and dipole–dipole interactions), all of which vary inversely as the intermolecular distance.[2−4] These favorable enthalpic interactions are, in part, offset by entropic penalties that arise from protein contraction with resultant rigidification. As ligand size increases, the degree of tightening of the interface required to maximize enthalpic interactions would require too high an entropic penalty, and enthalpy falls short of the maximum available. A diminished tightening produces less rigidification (and a diminished entropic penalty relative to that which would accompany maximum enthalpic

interaction). From the perspective of free energy, as ligand size increases, diminished favorable enthalpy (due to failure to maximize interactions) is compensated by a diminished entropic penalty (less rigidification).

Because there was no evidence of protein contraction or ligand-induced protein conformational change for carbonic anhydrase, Whitesides and co-workers attributed the entropic penalty to the ligand, that, when small, bound tightly to the protein interface and, upon elongation, associated more loosely with the protein binding site.[1] However, there is significant evidence that matrix metalloproteinases, particularly matrix metalloproteinase-3 (stromelysin-1), do undergo significant conformational change upon binding.[5−7] Such conformational changes raise the possibility that the protein itself could contract and rigidify around the ligand thereby tightening the protein–ligand interface. The thermodynamics would be the same as described by Whitesides and co-workers in the interfacial mobility model.[1]

While compelling in theory, experimental evidence for ligand-induced protein contraction as an underlying basis for enthalpy–entropy compensation is lacking. Calorimetric studies of the interaction of stromelysin-1 (matrix metalloproteinase 3) with the CGS 27023[8,9] series of ligands revealed significant enthalpy–entropy compensation as a function of ligand complexity (Figure 1). As with most instances of enthalpy–entropy compensation, the significance and origin of this observation were not readily apparent. A challenge in studying complex biological phenomena is that any single biochemical technique provides
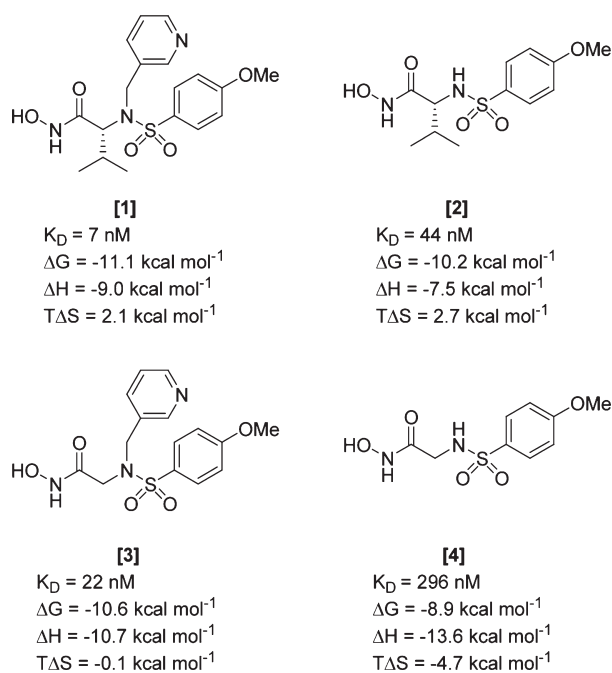
Figure 1. Structures and thermodynamics of ligand binding for CGS 27023 series ligands.

only a partial picture of the studied event. Although calorimetry provides accurate measures of K_{eq} and enthalpy, which can then be used to calculate free energy of binding and entropy, thermodynamic studies provide no structural insights. Crystallography provides a static view of molecular associations, but lacks insight into dynamic processes, that is, fast side chain motions, residual protein motion, periodic secondary structure changes, and global changes in physical properties upon binding. While dynamic NMR studies can provide insight into the former,[10−13] Raman spectroscopy can provide insight into global changes in the protein structure and microenvironment. As such, Raman spectroscopy represents a valuable, but underutilized, tool with which to probe key facets of protein ligand association.

Raman spectroscopy reports on vibrational modes of a molecule, and each vibration has a unique, characteristic signature. Thus, Raman spectroscopy can provide unique insights into changes in protein structure and, crucially for consideration of the interfacial mobility model, contraction. Unfortunately, Raman spectra are exceedingly complex, as each bond contributes to several vibrational modes. The challenge then becomes one of simplifying spectra such that useful information can be extracted; this simplification is most frequently accomplished by focusing on only a portion of the spectrum. Alternatively in Raman difference spectroscopy, the spectra of unbound protein and buffer are subtracted from that of the bound complex.[14−16] While the difference spectrum is dominated by ligand bands, protein bands are also observed, and these bands correspond to vibrational modes of the protein that are altered by ligand binding.[17,18] These Raman signatures yield insight into changes in secondary structure, side chain hydrogen bonding, side chain conformation, and, in the case of tryptophan, side chain environment.[14,19] Here, we utilize Raman difference spectroscopy in conjunction with both crystallographic and thermodynamic data to assess the validity of the interfacial mobility model in the case of stromelysin-1 ligand binding.

EXPERIMENTAL SECTION

Raman Microscopy. Raman spectra were acquired using a Raman microscope (Horiba JY, HR 800) operated by LabSpec5. The 632.8 nm output from a He−Ne laser (20 mW) is passed through an interference filter to eliminate the plasma lines of the laser. Subsequently, the output is reflected by a notch filter and directed toward the sample. The sample position and the laser focal point are adjusted by viewing a real-time video. The laser power at the sample is 6 mW, and the laser spot size is 2 μm. Raman signal is collected at 180° backscattering geometry by a 50× objective lens (NA, 0.75), passed through a notch filter to reject the Rayleigh line and directed through a 200 μm confocal hole. The signal passes through a 200 μm slit of the spectrograph (800 mm focal length) and is then then dispersed by an 1800 grooves/mm grating and detected by a CCD. The grating is calibrated by setting it to 0 nm using zeroth order white light and then to 520.7 cm^{-1} using the silicon band. The spectral resolution and wavenumber position repeatability are reported as 0.3 cm^{-1} at 680 nm and 1 pixel, which corresponds to 0.5 cm^{-1}, respectively.

Expression and Purification of Stromelysin-1. Stromelysin-1 catalytic domain (SCD) was expressed and purified as previously described.[20] Briefly, the nucleic acid sequence encoding amino acid residues 83−256 was cloned into the pET28b vector (Novagen); a stop codon was introduced in the reverse primer. The construct was expressed as inclusion bodies in *E. coli* BL-21(DE3)Gold cells and was purified using metal affinity chromatography. The purified protein was then dialyzed into the appropriate buffer (50 mM TrisHCl, pH 7.5, 10 mM CaCl$_2$, 1 μM Zn(OAc)$_2$).

Ligand Synthesis. All ligands utilized in these investigations were previously described using known synthetic techniques.[8,9,21] Full details can be found in the Supporting Information.

X-ray Crystallography. SCD was purified as described above, dialyzed into 2 mM TrisHCl, pH 7.5, 10 mM CaCl$_2$, and 1 μM Zn (OAc)$_2$, and lyophilized. After resuspension, a final purification step on a HiPrep 16/60 Sephacryl S-200 size exclusion column (Amersham Biosciences) was carried out. About 14 mg of the lyophilized enzyme powder was dissolved in 5 mL of buffer containing 2 mM TrisHCl, pH 7.5, 10 mM CaCl$_2$, and 1 μM Zn (OAc)$_2$ and loaded onto the column. SCD fractions eluted in 2 mM TrisHCl, pH 7.5, 10 mM CaCl$_2$, and 1 μM Zn (OAc)$_2$ were then checked for their purity by SDS-PAGE. Fractions containing pure SCD were pooled and concentrated (VIVASPIN 20, 3000 MWCO PES, Sartorius Stedim Biotech GmbH (SSB)) to 11.5 mg/mL. Prior to crystallization, SCD at a concentration of 11.5 mg/mL was centrifuged for 5 min at 4 °C. Either inhibitor **3** or **4** (dissolved in 100% dimethyl sulfoxide (DMSO) (Sigma)) was added to the protein solution to a final inhibitor concentration of 4 mM. The two samples were then incubated for 1−2 h at room temperature and centrifuged again. Crystallization experiments employed sitting-drop vapor diffusion at room temperature. Protein and mother liquor were mixed in a ratio of 1:1 (2.5 μL + 2.5 μL, reservoir volume 100 μL). Sealed plates were then incubated at 20 °C. Crystals large enough for diffraction experiments appeared after 1−4 weeks under the previously published conditions.[14]

Before data collection, crystals were cryoprotected in a solution containing 0.15 M ammonium sulfate, 0.1 M Na-cacodylate, pH 6.5, 30% PEG 8K, 4 mM inhibitor, and 10% PEG 400. X-ray data sets of SCD cocrystals, one in complex with inhibitor **3** and a second one complexed with compound **4**, were collected on the in-house RA-Micro 7 HFM Table Top Rotating Anode X-ray Generator (Rigaku) to 2.4 and 2.5 Å, respectively. The diffraction data were processed with HKL2000.[22] The catalytic domain of MMP-3 (pdb accession code 1b8y)[23] was used as a model for Molecular Replacement using PHASER.[24,25] The structures were refined with REFMAC5[26] with manual intervention with COOT[27] and validated using MOLPROBITY.[28] Dictionaries for the compounds were created by PRODRG.[15]

Protein Superimposition. The PDB files for SCD bound to nine ligands (1BM6, 2JT5, 1BQO, 2JNP, 1B3D, 2USN, 1B8Y), including SCD bound to **3** and **4**, were superimposed to apo SCD (1cqr) using Superpose[29] to minimize the global rmsd of C(α) atoms. The superimpositions were compared in PyMol,[30] and the distance between corresponding C(α) was measured for each bound structure relative to apo SCD. These values were entered into Microsoft Excel for additional data processing and graphical representations.

Raman Spectroscopy Samples. Compounds **1**−**4** were prepared as previously described.[8,9,21] 12.5 mM stocks of compounds **1**, **2**, **3**, and **4** were made in MeOH. The stock concentration was validated by titration against previously standardized protein. Protein was expressed and purified as described above and concentrated to 200−250 μM; concentrations were confirmed by the method of Edelhoch[31] using $\varepsilon_{280} = 27\,630$ M^{-1} cm^{-1}. Ligand was added in a 1:1 protein to ligand ratio, and additional MeOH was added to a final concentration of 2%. Samples were prepared within 24 h prior to obtaining Raman spectra.

Drop Coating Deposition Raman (DCDR). All experiments were performed at room temperature. For protein samples, 4 μL of a protein solution was deposited on a SpectRIM substrate, and water was evaporated without further treatment. The resulting deposit had a diameter of less than 2 mm. Raman spectra of protein samples were obtained by focusing the laser on the protein ring, which was approximately 50 μm away from the outer edge of the ring. The exposure time was 180 s for each spectrum, and six spectra were averaged for each sample. A buffer sample was prepared in the same manner. The buffer spectrum was obtained from the film-like portion of the deposit rather than the crystals formed around the center of the sample to achieve higher S/N. The exposure time was 10, and five spectra were averaged. Solid ligands were prepared by depositing 3 μL of methanol stock solutions on the SpectRIM substrate and evaporating the solvent. The exposure time was 15, and five spectra were averaged for each ligand.

Collection of Stromelysin-1 Complex Spectra. A difference spectrum that contains information of a bound ligand and changes in the protein conformation was obtained by subtraction of an apo protein spectrum from a spectrum of the complex (protein + ligand). The spectrum of the buffer was also subtracted or added because the contribution of buffer signals in each spectrum varies slightly (e.g., [difference] = [complex] − [apo protein]*f_1 − [buffer]*f_2, where f_1 and f_2 are scaling factors). Scaling factors for the apo protein and buffer spectra were chosen to achieve flat baselines. Positive bands can result from bound ligands, newly formed bonds, and changes in protein upon complexation. Negative bands can be due to loss or decrease in band intensity of existing protein bands upon ligand binding.

Difference spectra between spectra of complexes were obtained to determine the dependence of protein conformation changes on ligand structure (e.g., [difference] = [complex 1] − [complex 2]*f_1 − [buffer]*f_2), where f_1 and f_2 are scaling factors. The difference spectra were smoothed using a smoothing function in the Igor software package (Wavemetrics). A binomial algorithm and smoothing factor of 5 were used.

■ RESULTS AND DISCUSSION

Thermodynamics of Ligand Binding. While all ligands in the CGS 27023 series have been previously described,[8] the thermodynamics of binding were unknown. The free energy, enthalpy, entropy, and heat capacity of binding were determined by isothermal titration calorimetry. Heat capacity experiments were conducted at 15, 25, and 37 °C. Ligand binding was characterized in three buffers, MOPS, HEPES, and TRIS, to account for proton transfer events.[32] Observed enthalpies of binding were plotted against enthalpies of ionization. Linear regression was then used to determine the number of protons, *n*, transferred upon binding.

Table 1. Thermodynamics of Binding for Compounds 1−4[a]

	ΔG	ΔH_{bind}	$T\Delta S_{bind}$	ΔC_P
1	−11.1 ± 0.1	−9.0 ± 0.3	2.1 ± 0.3	−73 ± 7
2	−10.2 ± 0.1	−7.5 ± 0.4	2.7 ± 0.4	−74 ± 2
3	−10.6 ± 0.2	−10.7 ± 0.4	−0.1 ± 0.4	−69 ± 10
4	−8.9 ± 0.1	−13.6 ± 0.3	−4.7 ± 0.3	−60 ± 12

[a] ΔG, ΔH, and $T\Delta S$ are described in kcal mol^{-1}. ΔC_P is reported as cal mol^{-1} K^{-1}.

Because stromelysin-1 undergoes protonation of H224 upon binding,[5] it is critical to ensure that analyses are conducted with the actual thermodynamics of binding. In all cases, the calculated *n* was between 0.3 and 0.35 protons mol^{-1}, which is within the error of measurement. The derived thermodynamic parameters for binding are shown in Table 1.

Previously, enthalpy−entropy compensation has been rationalized by changes in protein or host hydration upon binding.[33,34] Fortunately, hydrophobic hydration affects ΔC_P in a predictable fashion. While changes in electrostatics or vibrational states of a protein during binding could, in principle, impact ΔC_P,[35] ΔC_P is the best available measurement of changes in solvent-exposed hydrophobic suface area and is therefore considered a hallmark of the hydrophobic effect.[36−38] The values of ΔC_P observed here, ranging from −60 to −74 cal mol^{-1} K^{-1}, show no evidence of changes in protein solvation upon binding. Additionally, there is no evidence that the presence of polar ligand functional groups accounts for the observed enthalpy−entropy compensation. Clearly, transfer of water from the protein to the ligand upon binding would contribute to the observed ΔC_P. However, if the transfer of water molecules from the protein surface to polar ligand functionalities contributed significantly to enthalpy−entropy compensation, such trends should correlate the presence or absence of a polar moiety. Compounds **1** and **3** contain a pyridyl group absent in compounds **2** and **4**. Nonetheless, compounds **1/2** and **3/4** have similar heat capacities and thermodynamic parameters. We therefore reject changes in protein solvation upon binding as an explanation for the observed thermodynamic parameters and will investigate a possible structural basis for enthalpy−entropy compensation in this system.

Determination of Protein−Ligand Crystal Structures. Both SCD complex structures for compounds **3** and **4** crystallized in the same space group with identical cell dimensions (see the Supporting Information). Unsurprisingly, both structures of SCD share the same fold as other previously reported SCD.[5,23,39−46] Superposition of the SCD structures in complex with inhibitors **3** and **4** gives an rmsd of 0.130 Å for 129 C(α) positions (Figure 2). Difference electron density for the inhibitors was visible in the first unbiased maps. The asymmetric unit of both structures is composed of one monomer, both of which are essentially complete apart from portions of the "long, flexible loop" (amino acids 210−234).[5] In the SCD structure complexed with inhibitor **3**, the electron density for amino acids 126, 213, 214, 218, 224, 231, 232, 237, 241, and 248 is weak; amino acids 215, 216, and 225−230 are absent. In the structure bound with compound **4**, the electron density for amino acids 213, 224, 231, 233, 236, 243, and 246−248 is poorly defined, while residues 215, 216, and 225−231 are completely disordered. Disordered amino acids within this flexible loop have been previously reported.[5,23,42] The positions and interactions of the catalytic
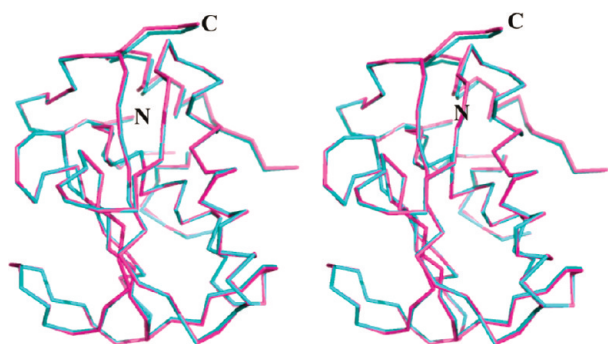
11517

dx.doi.org/10.1021/ja1098287 |*J. Am. Chem. Soc.* 2011, 133, 11515–11523

Figure 2. Stereo view of the C(α) tracing of SCDs complexed with inhibitors **3** (cyan) and **4** (magenta). This figure has been produced using PyMol.[30]

Figure 3. Stacked difference spectra for compounds **1**−**4**. Bands assigned to protein are labeled with the appropriate Raman shift. Unlabeled bands correspond to ligand shifts (unpublished results).

and structural Zn^{2+} and three Ca^{2+} ions are essentially identical in both complexes and consistent with previous reports.[5,23,39−46] One sulfate ion is also present in the SCD structures complexed with compounds **3** and **4** at the same position observed for SCD complexed with other nonpeptide inhibitors.[23]

Collection of Difference Spectra. Solution-phase Raman spectroscopy was not feasible because protein fluorescence following excitation at 568 nm obscured the Raman spectrum. Fortunately, drop coating deposition Raman (DCDR) generated useful spectra. Difference spectra containing information on protein vibrational changes upon binding were generated by ([complex] − [apo protein]*f). The scaling factor, f, is the multiplication factor required to match the intensity of the 1010 cm^{-1} phenylalanine band in the two subtracting spectra. A total of five spectra were collected for all bound complexes and unbound stromelysin-1 and averaged to yield the final spectra. To avoid complicating the spectra with unbound ligand, a 1:1 ratio of protein:ligand was used. On the basis of the previously determined K_D, this ratio resulted in a protein saturation greater than 99%. DCDR was also used to collect both pure ligand and buffer spectra to ensure only protein bands were included in the subsequent analysis (see the Supporting Information). The details of ligand band assignment will be discussed in a future publication. Table 2 summarizes the major protein peaks observed in all Raman spectra.

Newly Formed Bands. Three positive bands at 1386, 1072, and 894 cm^{-1} appear in all difference spectra between the apo protein and bound complexes (Figure 3). These bands do not correspond to any ligand modes or to bands observed in the apo protein spectrum. Further, these bands disappear when two
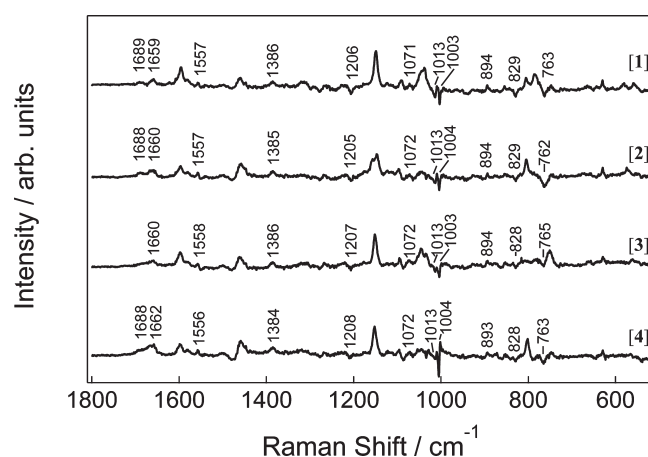
complex spectra are compared (Supporting Information). Additional experiments would be required to assign these bands unequivocally.

Ligand Binding Induces Changes in Secondary Structure. Raman spectroscopy is exquisitely sensitive to changes in protein secondary conformation. The main-chain backbone has 12 normal vibrational modes of which the amide I (carbonyl stretch) region is most commonly used to analyze secondary structure changes.[19,47] A positive band seen at 1660 cm^{-1} appears in all difference spectra for all protein complexes; a second positive feature at 1688 cm^{-1} is present in the difference spectra of protein−ligand complexes **1**, **2**, and **4**. While less obvious, the same feature near 1688 cm^{-1} is also seen in the difference spectrum of **3**. Both bands are assigned to correspond to random coil, which has multiple peaks across the entire amide I region. This conclusion is supported by crystallographic data, which show a universal decrease in α-helix and β-sheet structure upon binding and a compensatory increase in random coil features (Table 3).

Ligand Binding Changes the Local Environment of Tryptophan. Tryptophan is one amino acid that is particularly conducive to study by Raman spectroscopy as specific bands exist that characterize hydrogen bonding, side chain orientation, and hydrophobic environment.[19] In resonance Raman spectroscopy, UV excitation amplifies the tryptophan spectrum making them even more apparent. The ratio of the W7 fermi doublet of tryptophan (1340/1360 cm^{-1}) has been repeatedly validated as a marker of hydrophobicity in the tryptophan local

Table 2. Observed Difference Spectra Raman Shifts Assigned to Protein[19]

|	compound **1**	compound **2**	compound **3**	compound **4**
amide I, random coil	1689/1659	1688/1660	1660	1688/1660
tryptophan (W3)	1557	1557	1558/1550 (d)	1556
unassigned protein	1386 (br)	1385 (br)	1386 (br)	1386 (br)
tryptophan or phenylalanine	1206	1205	1207	1208
unassigned protein	1071	1072	1072	1072
tryptophan	1013	1013	1013	1013
phenylalanine	1003	1004	1003	1004
unassigned protein	894	894	894	893
tyrosine	829	829	828	828
tryptophan (W18)	763	762	765	763

Table 3. Changes in Secondary Structure for Compounds 1, 3, and 4 As Evidenced by X-ray Crystallography

compound	α-helix residues lost	β-sheet residues lost	random coil residues gained
1	−4	−2	+6
3	−6	−2	+8
4	−7	−2	+9

environment.[48−50] Unfortunately, attempts at solution-phase Raman spectroscopy were limited by sample fluorescence, and the Raman microscope available for DCDR did not have the option of UV excitation. Thus, the studies described here were limited to nonresonance Raman spectroscopy. In their initial report on the W7 band, Miuri and co-workers note that the ratio of the W7 doublet cannot be used with visible light excitation as CH aliphatic stretches overlap the 1340 cm^{-1} band.[50] Additionally, the 1360 cm^{-1} is not always discernible in nonresonance spectra,[51] even if readily apparent in the resonance Raman spectra.[48,49]

One structurally sensitive vibrational band in the nonresonance Raman spectroscopy of proteins is the W18 stretch (760 cm^{-1}), corresponding to the indole ring of tryptophan. Because the W18 stretch is among the most intense in the Raman spectrum, changes in intensity are readily detected, and the intensity of this band has been previously correlated to the number of hydrophobic contacts made by the indole ring. This deduction is based on work using the model compound, 3-methylindole. By measuring the W18 band intensity of 3-methylindole in solvents including H_2O, 1:1 H_2O:EtOH, EtOH, and pentane, Miura et al. demonstrated that the band intensity varied inversely with solvent hydrophobicity.[52] Because band intensity was comparable in vapor and aqueous spectra, Miura et al. concluded that an increased number of hydrophobic contacts on the indole ring resulted in a relatively decreased band intensity.[52] When considering the W18 band in difference Raman spectra where the spectrum of unbound protein is subtracted from that of bound protein, increased hydrophobic contacts on tryptophan in the bound state lead to the W18 band appearing as a negative feature. Figure 3 shows negative features in the difference spectra at ~760 cm^{-1} corresponding to the W18 stretch, indicating the presence of an increased number of hydrophobic contacts in the bound state.

There is a significant temptation to analyze the relative intensities of the various W18 ligand bands through the generation of a double difference spectrum. One must, however, exercise caution as any error in the initial Raman spectra has been significantly propagated as two difference spectra were generated. Assuming a 5% error in the initial measurements (inclusive of buffer subtraction), propogation of errors indicates that the error in the difference spectra is 7%. Generation of a double difference spectra would further increase the error to 10%. To determine if any reliable trends in relative W18 band intensities were present, a series of double displacement spectra were generated (Supporting Information Figures S6 and S7). Unfortunately, these spectra yielded unreliable and, at times, contradictory results, likely due to the small variations in peak intensity and the substantial error associated with generating double difference spectra. To ascertain trends among ligands, nondifference Raman spectroscopy will have to be combined with other high resolution techniques, such as isothermal titration calorimtery X-ray crystallography or NMR protein structure determinations.
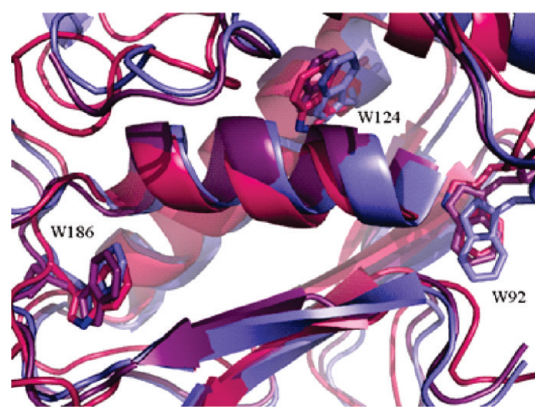
Figure 4. Conformation of the three internal tryptophans of unbound SCD (pink), SCD bound to **1** (blue), and SCD bound to **4** (purple).

Table 4. Conformations of Stromelysin-1 Catalytic Domains[a]

	W92			W124			W186		
	C(α)	C1	$X^{1,2}$	C(α)	C1	$X^{1,2}$	C(α)	C1	$X^{1,2}$
1	1.58 Å	1.18 Å	17.3°	1.17 Å	1.1 Å	1.1°	1.22 Å	1.27 Å	2.3°
3	0.20 Å	0.20 Å	6.1°	0.21 Å	0.19 Å	2.7°	0.08 Å	0.15 Å	0.1°
4	0.28 Å	0.28 Å	8.7°	0.18 Å	0.18 Å	4.5°	0.22 Å	0.22 Å	0.3°

[a] Distances for C(α) and C(1) are the measured distance between the unbound crystal structure 1CQR with the superimposed bound complex. RMS of C(α) for superimposition of apo with compounds **3** and **4** was 0.63; RMS of C(α) for superimposition of apo with compound **1** was 3.75. Value for $\chi^{1,2}$ dihedral is the change in the dihedral upon ligand binding.

Despite this limitation, nondifference Raman spectroscopy does provide clear evidence that the number of hydrophobic contacts within the protein interior of stromelysin-1 increases upon ligand binding. Additionally, this technique is reasonably accessible and does not require protein crystals, which can be difficult to obtain. There are two ways in which interior tryptophans could experience increased hydrophobic contacts, residue translocation or protein contraction with increased packing of the protein interior.

We first consider the possibility of tryptophan translocation. X-ray crystallographic data show no major change of tryptophan conformation upon ligand binding (Figure 4). For tryptophan translocation to account for the observed W18 band, the translocation must differ significantly between compounds **1** and **4** because the W18 band is much stronger for both compounds **3** and **4** than for compound **1**. Table 4 shows the change in position of C(α) and C1 and the $\chi^{1,2}$ from apo protein. While the $\chi^{1,2}$ angle for W92 does change significantly upon binding, the change is consistent across the series. Also, compound **1** exhibits the largest change in W92 $\chi^{1,2}$ dihedral angle but the smallest change in W18 intensity upon ligand binding. These small changes in $\chi^{1,2}$ dihedral are also evidenced by the W3 tryptophan stretch in all difference spectra. Thus, the structural data show no evidence for translocation.

Protein contraction would also increase the number of hydrophobic contacts on tryptophan. Because proteins contain intraprotein voids[53−57] and have average interior surface complementarities of only 60−80%,[58,59] contraction is feasible. An analysis of 50 protein structures demonstrated that most buried

tryptophans only have ~60% surface complementarity (surface area contacted by another amino acid residue); 40% of the tryptophan surface lacks any hydrophobic contacts.[58,59] Lysozyme is a protein for which ligand binding and protein contraction were convincingly linked using both volume and intrinsic compressibility measurements.[60] Ligand binding by lysozyme also decreases the W18 mode intensity and led to negative features at ~760 cm^{-1},[52] which could be contributed to by protein contraction. While direct correlation of the W18 band with protein contraction has not, to our knowledge, been reported in the literature, supporting data have, in fact, been published by several groups independently. In his 2004 review of protein contraction/expansion as a driving force for binding and enthlapy—entropy compensation, Dudley Williams and co-workers described two model systems, avidin—biotin and hemoglobin—oxygen.[61] Avidin—biotin binding is a representative system of protein contraction. Using H/D exchange of amide backbone proteins characterized by MALDI, binding of biotin by avadin led to a marked decrease of H/D exchange of the protein backbone, which was interpreted as increased protein packing and therefore decreased access of D_2O to the amide protons.[62] Thermodynamically, binding of biotin and avadin demonstrates a marked enthalpic benefit and entropic penalty of binding.[63,64] This system has also been studied by difference resonance Raman spectroscopy to analyze changes in the local tryptophan environments upon binding. Both the W7 and the W18 bands experienced an increase in intensity indicative of an increase in local hydrophobicity about the indole ring.[65] In conglomeration, these results support the use of the W18 band as a marker for protein contraction.

Similarly, when investigating protein expansion as demonstrated by hemoglobin binding to oxygen, the converse finding is obtained.[61] Hb exists in two forms in the blood, a "tense" rigid state having a low affinity for O_2 and a high affinity "relaxed" state that avidly binds both O_2.[66] Using H/D exchange and ESI experiments, Williams and co-workers demonstrated that transitioning from a tense to relaxed state upon binding O_2 resulted in increased H/D exchange and protein expansion.[62] Subsequent binding events lead to relaxation of additional subunits until the protein is fully relaxed after binding of the fourth O_2 molecule. Thermodynamically, this phenomena was entropically driven and entropically opposed, with each successive binding event resulting in a smaller entropic benefit and enthalpic penalty of binding.[67,68] The concept of protein expansion is also supported spectroscopically by analyzing work by Nagatomo et al.,[69] which showed decreased hydrophobicity of tryptophans using the W18 band upon carbon monoxide binding. Because this was a non-resonance study, the tryptophan spectra are not enhanced, and the 1360 cm^{-1} peak is not readily visible for analysis. Carbon monoxide is more facile to use for spectroscopic experiments as its higher affinity results in a more stable complex. Nonetheless, the binding site and binding mode are conserved, and protein dynamics should be conserved in both cases.

Ideally, our Raman spectroscopy work would be supplemented by physical measurements of intrinsic compressibility, but these require crystals that we were unable to acquire. Nonetheless, either tryptophan translocation or protein contraction must occur to produce the W18 observations in these studies, and data supporting translocation were lacking. This lack of evidence for translocation combined with the previous correlation of decreased W18 band and protein volume for lysozyme leads us to the conclusion that protein contraction is responsible for the increased hydrophobic contacts on tryptophan.
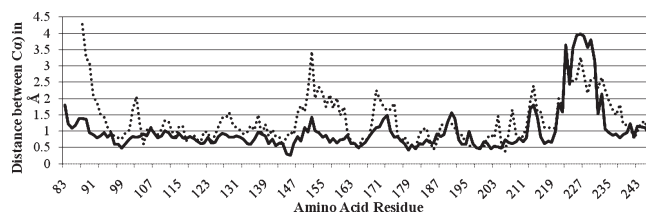

Figure 5. Average variation of C(α) upon ligand binding. Based on protein superimposition of PDB files 1BM6, 2JT5, 1BQO, 2JNP, 1B3D, 2USN, 1B8Y, and the crystal structures described herein. Solid line depicts ligands binding only the S1′ hydrophobic pocket and catalytic zinc. Dashed line depicts larger ligands binding additional subpockets.

Consideration of the Interfacial Mobility Model. The interfacial mobility model postulates that high affinity ligand binding results from tightening of the protein—ligand interface, which in the case of stromelysin-1, we propose arises from protein contraction about the ligand. Consequences of protein contraction would include increased internal protein packing, rigidification, and decreased residual movement. Thermodynamically, the interfacial mobility model manifests with an enthalpic benefit and entropic penalty of binding that is inversely proportional to ligand complexity. While it is currently impossible to deconvolute accurately and reliably the contribution of van der Waals interactions and hydrogen bonding to binding enthalpy, there has been success in correlating entropies of binding to either residual protein motion or residual entropy.[70,71] As both decreased residual protein movement and increased internal packing are consequences of protein contraction, we correlate our Raman observations of internal packing (Figure 3), and therefore contraction and decreased residual protein motion, with the experimental entropies of binding (Figure 1).

In the case of compounds **1** and **2**, both enthalpy and entropy contribute to ligand binding, and the magnitude of entropic contribution is comparable (2.1 and 2.7 kcal mol^{-1}, respectively). Entropy does not contribute significantly for binding of compound **3** (-0.1 kcal mol^{-1}), but a significant entropic penalty of binding occurs for compound **4** (-4.7 kcal mol^{-1}). On the basis of these thermodynamic observations, the interfacial mobility model predicts that compounds **1** and **2** would experience relatively small and comparable contractions as they have comparable entropies of binding. Binding of compound **3** should cause a protein contraction greater than that for compounds **1** and **2** but less than for compound **4**.

While internal packing, as demonstrated by the W18 tryptophan band, is one proxy for protein contraction, a second proxy marker for this phenomenon is decreased residual movement. Additionally, X-ray crystallography is high resolution and likely to yield insights into minor differences between ligands. To this end, an analysis of crystal structures was undertaken.[5,6,23,39,45,72] Ten solved bound structures, including those for compounds **1**, **3**, and **4**, were superimposed with apo SCD using SuperPose,[29] and the difference between C(α) positions for apo- and holoprotein was measured for all residues. These results are plotted graphically in Figure 5. The average difference in C(α) position across all residues and structures is approximately 1 Å. There are, however, certain protein regions where the difference C(α) is much greater, and these regions correspond to random coil secondary structure. All structures demonstrate increased variability of C(α) position for the loop encompassing residues 221—233.

Interestingly, two loops (150−160 and 170−175) demonstrate an increased difference of C(α) position variability for large ligands, as defined by binding more than just the S1′ and Zn^{2+} subpockets,
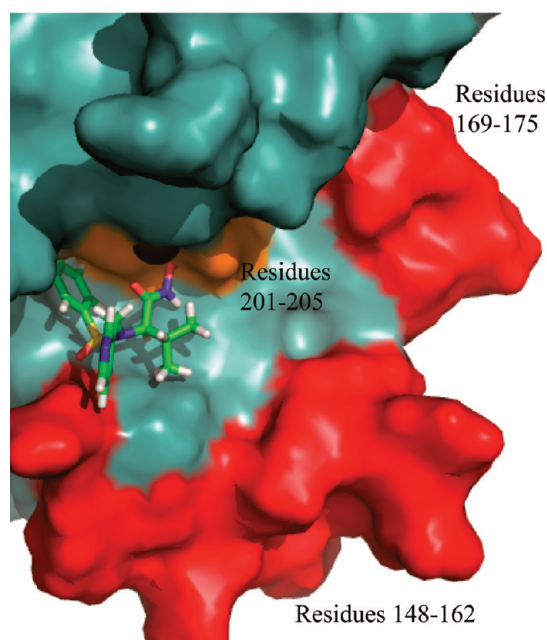

Figure 6. Regions of variable mobility for SCD upon ligand binding. Regions depicted in red show a clear increase in mobility when SCD is bound to large ligands. Regions depicted in orange show a trend toward increased mobility when bound to large ligands.

versus small ligands that bind only the S1′ and Zn^{2+} subpockets. The average difference in C(α) for large as compared to small ligands is 0.9 ± 0.2 versus 2.0 ± 0.5 Å for residues 148−161, respectively. Similarly, the average difference in C(α) for residues 169−175 is 1.1 ± 0.2 versus 1.8 ± 0.3 Å, respectively, for large and small ligands. It is intriguing that these regions in relatively close proximity to the active site (Figure 6) demonstrate increased variability in C(α) large relative to small ligands as this could reflect decreased residual movement of these residues. If C(α) variability between superimposed protein structures truly reflects residual protein motion, this would further support the interfacial mobility model.

We have presented data that protein contraction, as judged by the W18 Raman band, varies inversely with ligand complexity. Additionally, crystallographic analysis reveals reduced motions in two loops and possibly an α-helix near the active site upon binding of high affinity small ligands. The W18 Raman band indicates that for compounds **1** and **2**, the protein contracts identically even though **2** lacks the pyridyl substituent. Similarly, compounds **3** and **4** behave similarly despite the difference of pyridyl moiety. Figure 7 shows the subpockets of the SCD active site. The majority of subpockets are composed of multiple secondary features. The S1′ hydrophobic pocket is made up of a loop (residues 218−222) and an α helix (residues 195−201). The S1 groove is formed by a loop (residue 163) and β sheet (residue 165−166); that same loop also forms the P1 groove (residues 162, 164). Thus, while lacking the pyridyl moiety ring, compound **2** still contacts the P1 loop through binding of its isopropyl group. Although compound **3** contains the pyridine moiety, the structure reveals that this substituent is rotated away from the P1 groove. Thus, compounds **1** and **2** contact the same secondary features; the same observation is true for compounds
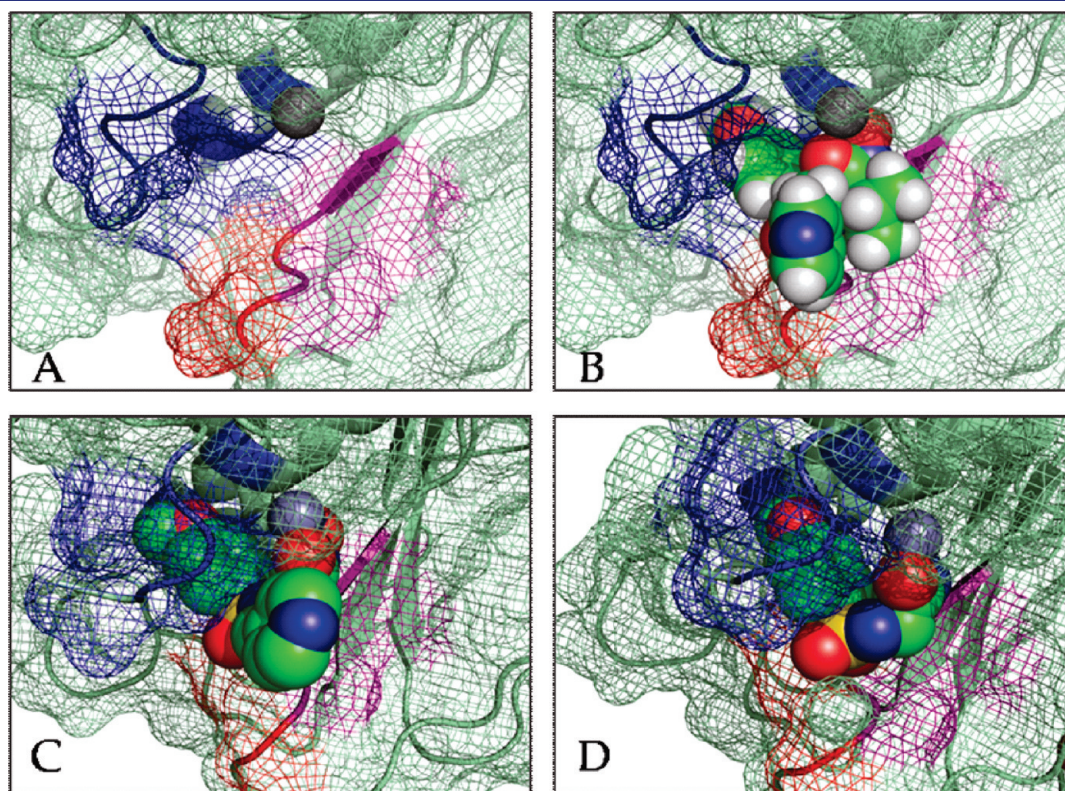

Figure 7. Meshwork structures of SCD subpockets. (A) Empty meshwork of SCD. S1′ pocket is in blue, P1 groove is in red, and S1 groove is in purple. (B) Meshwork of bound compound **1**. (C) Meshwork of bound compound **3**. (D) Meshwork of bound **4**.

3 and 4. The *p*-methoxyphenyl group for compounds 3 and 4 interacts more extensively with the protein than seen in compound 1. This could result in tightening of the S1′—ligand interface around the smaller ligands.

When Krishnamurthy et al. first described the interfacial mobility model, they defined ligand size as the number of "distal residues" contacted.[1] In the context of human carbonic anhydrase, the distal residues were amino acids at an increased distance from the catalytic zinc in the conical active site. Because SCD has an active site groove, we originally thought to define ligand size as a function of subpockets occupied. This assumption is flawed because small changes in ligand structure can dramatically alter the binding mode; that is, the absence of the isopropyl moiety allowed reorientation of the pyridyl moiety in the active site. While a priori we had expected to see a linear trend in protein contraction, this ligand rearrangement in the active site caused compound pairs 1/2 and 3/4 to give similar results despite possessing moieties that could have bound additional subpockets. The small ligands 3/4 bind loop 218—222 and α-helix 195—201 in addition to the catalytic zinc. The large ligands 1/2 interact with these residues as well as loop 162—164 and β-sheet 165—166. Once "ligand size" was defined by the secondary structural elements involved in ligand binding, which correlates closely with residues contacted, the degree of protein contraction correlates well with "ligand size". Thus, trends in protein contraction and thermodynamics are in good accord with those predicted by the interfacial mobility model.[1]

CONCLUSIONS

The combination of results from thermodynamic data, crystallography, and Raman spectroscopy presented here provides consistent experimental support for the interfacial mobility model for the binding of the CGS ligand series to stromelysin-1. Additional work is needed in a variety of protein systems to verify the generality of these findings. Two potential models are FK-506 binding protein (FKBP) and Src-SH2 domain as both proteins contain a single tryptophan moiety. In the case of FKBP, the tryptophan is located at the seat of the hydrophobic pocket; the tryptophan for the Src-SH2 domain is buried deep within the protein interior.

ASSOCIATED CONTENT

ⓢ Supporting Information. Complete refs 8 and 41, detailed ligand synthesis and X-ray crystallography refinement details, protein superimposition data, and supporting Raman spectra. This material is available free of charge via the Internet at http://pubs.acs.org.

AUTHOR INFORMATION

Corresponding Author
gustafson.5@osu.edu

ACKNOWLEDGMENT

REFERENCES

(1) Krishnamurthy, V. M.; Bohall, B. R.; Semetey, V.; Whitesides, G. M. *J. Am. Chem. Soc.* **2006**, *128*, 5802.

(2) Hornig, J. F.; Hirschfelder, J. O. *J. Chem. Phys.* **1952**, *20*, 1812.

(3) London, F. *Z. Phys.* **1930**, *63*, 245.

(4) Margenau, H. *J. Chem. Phys.* **1938**, *6*, 896.

(5) Chen, L.; Rydel, T. J.; Fei, G.; Dunaway, C. M.; Pikul, S.; Dunham, K. M.; Barnett, B. L. *J. Mol. Biol.* **1999**, *293*, 545.

(6) Li, Y.-C.; Zhang, Z.; Melton, R.; Ganu, V.; Gonnella, N. C. *Biochemistry* **1998**, *37*, 14048.

(7) Parker, M. H.; Ortwine, D. F.; O'Brien, P. M.; Lunney, E. A.; Banotai, C. A.; Mueller, W. T.; McConnell, P.; Brouillette, C. G. *Bioorg. Med. Chem. Lett.* **2000**, *10*, 2427.

(8) MacPherson, L. J.; et al. *J. Med. Chem.* **1997**, *40*, 2525.

(9) MacPherson, L. J.; Parker, D. T. A61K031-44; Ciba-Geigy Corp.: U.S., 1997; US 5646167, p 31.

(10) Lindorff-Larsen, K.; Best, R. B.; DePristo, M. A.; Dobson, C. M.; Vendruscolo, M. *Nature* **2005**, *433*, 128.

(11) Philippopoulos, M.; Lim, C. *Proteins: Struct., Funct., Bioinf.* **1999**, *36*, 87.

(12) Wand, A. J. *Nat. Struct. Biol.* **2001**, *8*, 926.

(13) Yao, J.; Eliezer, D.; Wright, P. E.; Dyson, H. J. *Biochemistry* **2001**, *40*, 3561.

(14) Chen, D. H.; Rhee, K. W.; Martin, C.; Sloan, D.; Callender, R.; Yue, K. T. *Biophys. J.* **1987**, *51*, A311.

(15) Deng, H.; Pande, C.; Callender, R. H.; Ebrey, T. G. *Photochem. Photobiol.* **1985**, *41*, 467.

(16) Kakitani, H.; Kakitani, T.; Rodman, H.; Honig, B.; Callender, R. *J. Phys. Chem.* **1983**, *87*, 3620.

(17) Callender, R.; Deng, H. *Annu. Rev. Biophys. Biomol. Struct.* **1994**, *23*, 215.

(18) Callender, R.; Deng, H.; Gilmanshin, R. *J. Raman Spectrosc.* **1998**, *29*, 15.

(19) *Proteins: Structure, Function, and Engineering*; Biswas, B. B., Roy, S., Eds.; Plenum Press: New York, 1995; Vol. 24.

(20) Wilfong, E. M.; Locklear, U. N.; Toone, E. J. *Bioorg. Med. Chem. Lett.* **2010**, *20*, 280.

(21) Fei, X.; Zheng, Q. H.; Hutchins, G. D.; Liu, X.; Stone, K. L.; Carlson, K. A.; Mock, B. H.; Winkle, W. L.; Glick-Wilson, B. E.; Miller, K. D.; Fife, R. S.; Sledge, G. W.; Sun, H. B.; Carr, R. E. *J. Labelled Compd. Radiopharm.* **2002**, *45*, 449.

(22) Minor, W.; Cymborowski, M.; Otwinowski, Z. *Acta Phys. Pol., A* **2002**, *101*, 613.

(23) Pavlovsky, A. G.; Williams, M. G.; Ye, Q. Z.; Ortwine, D. F.; Purchase, C. F., II; White, A. D.; Dhanaraj, V.; Roth, B. D.; Johnson, L. L.; Hupe, D. J.; Humblet, C.; Blundell, T. L. *Protein Sci.* **1999**, *8*, 1455.

(24) McCoy, A. J.; Grosse-Kunstleve, R. W.; Storoni, L. C.; Read, R. J. *Acta Crystallogr., Sect. D* **2005**, *61*, 458.

(25) Storoni, L. C.; McCoy, A. J.; Read, R. J. *Acta Crystallogr., Sect. D* **2004**, *60*, 432.

(26) Murshudov, G. N.; Vagin, A. A.; Dodson, E. J. *Acta Crystallogr., Sect. D* **1997**, *53*, 240.

(27) Emsley, P.; Cowtan, K. *Acta Crystallogr., Sect. D: Biol. Crystallogr.* **2004**, *60*, 2126.

(28) Davis, I. W.; Murray, L. W.; Richardson, J. S.; Richardson, D. C. *Nucleic Acids Res.* **2004**, *32*, W615.

(29) Maiti, R.; Van Domselaar, G. H.; Zhang, H.; Wishart, D. S. *Nucleic Acids Res.* **2004**, *32*, W590.

(30) DeLano, W. L. DeLano Scientific: Palo Alto, CA, 2007.

(31) Edelhoch, H. *Biochemistry* **1967**, *6*, 1948.

(32) Christensen, T.; Gooden, D. M.; Kung, J. E.; Toone, E. J. *J. Am. Chem. Soc.* **2003**, *125*, 7357.

(33) Grunwald, E.; Steel, C. *J. Am. Chem. Soc.* **1995**, *117*, 5687.

11522

dx.doi.org/10.1021/ja1098287 |*J. Am. Chem. Soc.* 2011, 133, 11515–11523

(34) Leung, D. H.; Bergman, R. G.; Raymond, K. N. *J. Am. Chem. Soc.* **2008**, *130*, 2798.

(35) Sturtevant, J. M. *Proc. Natl. Acad. Sci. U.S.A.* **1977**, *74*, 2236.

(36) Spolar, R. S.; Record, M. T. *Science* **1994**, *263*, 777.

(37) Murphy, K. P.; Freire, E. *Adv. Protein Chem.* **1992**, *43*, 313.

(38) Livingstone, J. R.; Spolar, R. S.; Record, M. T. *Biochemistry* **1991**, *30*, 4237.

(39) Alcaraz, L. A.; Banci, L.; Bertini, I.; Cantini, F.; Donaire, A.; Gonelli, L. *J. Biol. Inorg. Chem.* **2007**, *12*, 1197.

(40) Becker, J. W.; Marcy, A. I.; Rokosz, L. L.; Axel, M. G.; Burbaum, J. J.; Fitzgerald, P. M. D.; Cameron, P. M.; Esser, C. K.; Hagmann, W. K.; Hermes, J. D.; Springer, J. P. *Protein Sci.* **1995**, *4*, 1966.

(41) Cheng, M.; et al. *J. Med. Chem.* **2000**, *43*, 369.

(42) Dhanaraj, V.; Ye, Q. Z.; Johnson, L. L.; Hupe, D. J.; Ortwine, D. F.; Dubar, J. B.; Rubin, J. R.; Pavlovsky, A.; Humblet, C.; Blundell, T. L. *Structure* **1996**, *4*, 375.

(43) Dunten, P.; Kammlott, U.; Crowther, R.; Levin, W.; Foley, L. H.; Wang, P.; Palermo, R. *Protein Sci.* **2001**, *10*, 923.

(44) Kohno, T.; Hochigai, H.; EYamashita, E.; Tsukihara, T.; Kanaoka, M. *Biochem. Biophys. Res. Commun.* **2006**, *344*, 315.

(45) Pikul, S.; McDow Dunham, K. L.; Almstead, N. G.; De, B.; Natchus, M. G.; Anastasio, M. V.; McPhail, S. J.; Snider, C. E.; Taiwo, Y. O.; Rydel, T.; Dunaway, C. M.; Gu, F.; Mieling, G. E. *J. Med. Chem.* **1998**, *41*, 3568.

(46) Steele, D. L.; El-Kabbani, O.; Dunten, P.; Windsor, L. J.; Kammlott, R. U.; Crowther, R. L.; Michoud, C.; Engler, J. A.; Birktoft, J. J. *Protein Eng.* **2000**, *13*, 397.

(47) *Infrared and Raman Spectroscopy*; Schrader, B., Ed.; VCH Verlagsgesellschaft mbH: Weinheim, 1995.

(48) Ettrich, R.; Brandt, W.; Kopecky, V.; Baumruk, V.; Hofbauerova, K.; Pavlicek, Z. *Biol. Chem.* **2002**, *383*, 1667.

(49) Fujimoto, N.; Toyama, A.; Takeuchi, H. *Biopolymers* **2002**, *67*, 186.

(50) Miura, T.; Takeuchi, H.; Harada, I. *Biochemistry* **1988**, *27*, 88.

(51) Efremov, R. G.; Feofanov, A. V.; Nabiev, I. R. *J. Raman Spectrosc.* **1992**, *23*, 69.

(52) Miura, T.; Takeuchi, H.; Harada, I. *Biochemistry* **1991**, *30*, 6074.

(53) Chothia, C. *Annu. Rev. Biochem.* **1984**, *53*, 537.

(54) Rashin, A. A.; Iofin, M.; Honig, B. *Biochemistry* **1986**, *25*, 3619.

(55) Rasper, J.; Kauzmann, W. *J. Am. Chem. Soc.* **1962**, *84*, 1771.

(56) Richards, F. M. *Annu. Rev. Biophys. Bioeng.* **1977**, *6*, 151.

(57) Vanderkooi, J. M. *Biochim. Biophys. Acta, Protein Struct. Mol. Enzymol.* **1998**, *1386*, 241.

(58) Banerjee, R.; Ray, S.; Bhattacharya, D. *Curr. Sci.* **2000**, *78*, 258.

(59) Banerjee, R.; Sen, M.; Bhattacharya, D.; Saha, P. *J. Mol. Biol.* **2003**, *333*, 211.

(60) Gekko, K.; Yamagami, K. *Chem. Lett.* **1998**, 839.

(61) Williams, D. H.; Stephens, E.; O'Brien, D. P.; Zhou, M. *Angew. Chem., Int. Ed.* **2004**, *43*, 6596.

(62) Williams, D. H.; Stephens, E.; Zhou, M. *J. Mol. Biol.* **2003**, *329*, 389.

(63) Hyre, D. E.; Le Trong, I.; Freitag, S.; Stenkamp, R. E.; Stayton, P. S. *Protein Sci.* **2000**, *9*, 878.

(64) Weber, P. C.; Wendoloski, J. J.; Pantoliano, M. W.; Salemme, F. R. *J. Am. Chem. Soc.* **1992**, *114*, 3197.

(65) Clarkson, J.; Sudworth, C.; Masca, S. I.; Batchelder, D. N.; Smith, D. A. *J. Raman Spectrosc.* **2000**, *31*, 373.

(66) Fersht, A. R. *Structure and Mechanism in Protein Science*; W. H. Freeman and Co.: New York, 1999.

(67) Colosimo, A.; Coletta, M.; Falcioni, G.; Giardina, B.; Gill, S. J.; Brunori, M. *J. Mol. Biol.* **1982**, *160*, 531.

(68) Johnson, C. R.; Ownby, D. W.; Gill, S. J.; Peters, K. S. *Biochemistry* **1992**, *31*, 10074.

(69) Nagatomo, S.; Nagai, M.; Shibayama, N.; Kitagawa, T. *Biochemistry* **2002**, *41*, 10010.

(70) Fredrick, K. K.; Marlow, M. S.; Valentine, K. G.; Wand, A. J. *Nature* **2007**, *448*, 325.

(71) Stockmann, H.; Bronowska, A.; Syme, N. R.; Thompson, G. S.; Kalverda, A. P.; Warriner, S. L.; Homans, S. W. *J. Am. Chem. Soc.* **2008**, *130*, 12420.

(72) Finzel, B. C.; Baldwin, E. T.; Bryant, G. L.; Hess, G. F.; Wilks, J. W.; Trepod, C. M.; Mott, J. E.; Marshall, V. P.; Petzold, G. L.; Poorman, R. A.; O'Sullivan, T. J.; Schostarez, H. J.; Mitchell, M. A. *Protein Sci.* **1998**, *7*, 2118.